Journal of Polymers and the Environment (2019) 27:148–157
https://doi.org/10.1007/s10924-018-1330-4

ORIGINAL PAPER

Producing Conductive Graphene–Nanocellulose Paper in One-pot

Ruibin Wang[1,2] · Qianli Ma[1,2] · Huilong Zhang[3] · Zhengqiang Ma[3] · Rendang Yang[1] · J. Y. Zhu[2]

Published online: 8 November 2018

Abstract
This paper reports a facile one-pot method to produce graphene oxide nanocellulose composite (GNCC) that was subsequently reduced using L-ascorbic acid to form a conductive paper (CP). Cellulose fibers were directly added into the reaction system during graphite exfoliation using sulfuric acid to produce cellulose nano- or microfibrils through acid hydrolysis along with mechancial mixing. FTIR and Raman analyses indicated that reduction using L-ascorbic acid efficiently produced a well-deoxygenated CP with high conductivity of 116.3 ± 1.5 S m^{-1} at 20% graphene oxide loading. Furthermore, the presence of cellulose nano- or microfibrils improved CP thermal stability with onset degradation T_{onset} of 319 °C as well as mechanical properties with a specific tensile of 19 N mg^{-1}. This one-pot method substantially simplified the GNCC production process and has practical significance.

Keywords One-pot · Graphene oxide · Cellulose · Conductive paper · Thermal stablility

Introduction

Flexible electronics have received great interests recently in emerging fields such as portable micropower devices, smart textiles, and implantable biosensors [1, 2]. Graphene–cellulose or graphene–nanocellulose composite (GCC or GNCC) stands out for its dimensional designability [3, 4]. Furthermore, GCC or GNCC inherits the properties of both graphene, being highly conductive, and cellulose, being of light weight and biodegradable. Furthermore, GCC or GNCC can be made as paper like freestanding materials for various applications [5].

Currently, GCC or GNCC is fabricated through (1) separate synthesis of cellulose or nanocellulose and graphene (or their derivatives), followed by (2) coating, blending, in situ polymerization, or doping to form an uniform intermediate, and (3) further transforming the intermediate into a final composite product [6, 7]. Often, the process needs to be operated under elevated temperatures and pressures [4, 8–10]. This undoubtedly impedes the production scalability. An efficent process for producing GCC or GNCC is needed. The production of cellulose nanomaterials itself is energy intensive when using pure mechanical fibrillation [11]. Chemical treatments [12–14] can reduce energy input for fibrillation. Acid hydrolysis has been extensively used as an effective chemical treatment for producing cellulose nanomaterials [15]. Specifically, concentrated sufuric acid hydrolysis in the cocentration range of between 40 and 65 wt% at approximately 40–60 °C for 60 min has been extensively used to produce cellulose nanocrystals (CNC) from wood fibers since 1940s [16–21]. We found that under slighly mild hydrolysis conditions using concentrated sufuric acid, under-hydrolyzed cellulosic fibers can be easily fibrillated into cellulose nanofibrils (CNF) [21, 22]. On the other hand, concentrated sulfuric acid has almost exclusively been used for the production of graphene, as described in the classic method by Hummers and Offeman [23]. The typical reaction condition, i.e., 98 wt% acid concentration between 35 and 90 °C for approximately 60 min in this classic method are not far from that those typically used for producing cellulose nanocrystals. It is

Electronic Supplementary Material The online version of this article (https://doi.org/10.1007/s10924-018-1330-4) contains supplementary material, which is available to authorized users.

✉ J. Y. Zhu
jzhu@fs.fed.us

[1] State Key Laboratory of Pulp and Paper Engineering, South China University of Technology, Guangzhou 510640, China

[2] Forest Products Laboratory, U. S. Forest Service, U. S. Department of Agriculture, Madison, WI 53736, USA

[3] Department of Electrical and Computer Egineering, University of Wisconsin-Madison, Madison, WI 53705, USA

therefore feasible and advantageous to use concentrated sulfuric acid hydrolysis for producing both nanocellulose and graphene simutaneously in one pot.

Here we report, for the first time, a facile one-pot process to produce GNCC that is subsequently reduced using L-ascorbic acid to form a conductive paper (CP) with great conductivity. In this process, cellulose nano- or microfibrils were produced in-situ during graphite exfoliation in one pot by concentrated sulfuric acid to form a promising intermediator GNCC, without separately synthesizing graphene and nanocellulose as practiced in almost all reported studies [6, 7]. This one-pot process was conceptualized based on our prior studies that CNC and CNF can be produced from wood fibers under concentrated sulfuric acid hydrolysis conditions with mechanical fibrillation [21, 22]. Instead of producing nanocellulose using a separate process, we hypothesize that cellulose nano- or microfibrils can be produced in-situ from cellulosic fibers under the condition for graphene exfoliation using concentrated sulfuric acid hydrolysis and potassium permanganate oxidation with mechanical mixing. The presence of CNF in the GNCC suspension validated our hypothesis. Furthermore, green reducing agent L-ascorbic acid was employed to efficiently reduce GNCC to reduced GNCC (RGNCC), which was further ultra-filtrated to produce a highly conductive, thermally stable, and freestanding CP. This one-pot process offers substantial advantages for producing graphene-cellulose based CP applicable in flexible electronics.

Experimental

Materials

Graphite (99.95% metals basis, 8000 mesh) was supplied by Aladdin Industrial Corporation (Shanghai, China). Bleached eucalyptus pulp (BEP) fibers were obtained by disintegrating dry lap of commercial eucalyptus kraft pulp (Aracruz Cellulose, Brazil) as described previously [13].

All chemicals were of ACS reagent grade and purchased from Sigma-Aldrich (St. Louis, MO). The Millipore PVDF membrane used for ultrafiltration (Durapore membrane filters, 0.22 µm pore size, 142 mm diameter) was purchased from Fisher Scientific (Pittsburgh, PA).

One-pot Synthesis of GNCC

The one-pot GNCC synthesis process, schematically shown in Fig. 1a, is a modification of the Hummers method [23]. Briefly, 0.5 g of graphite and 0.25 g of sodium nitrate were both slowly mixed into 11.5 mL of concentrated sulfuric acid (98 wt%) in a 250-mL flask in the ice bath (0 °C) with light agitation using a stirrer. Then 1.5 g of potassium permanganate was gradually added while agitating. After 15 min, the ice bath was removed and the flask was heated to 35 ± 3 °C and maintained for 30 min. Subsequently, 17.25, 23.00, or 28.75 mL of de-ionized (DI) water was carefully added drop-wise over 15 min, which reduced the concentration of sulfuric acid to approximately 55 wt%, 48 wt%, and 42 wt% (lower than those used for typical cellulose nanocrystal production), respectively, before heating the flask to 50 or 60 °C

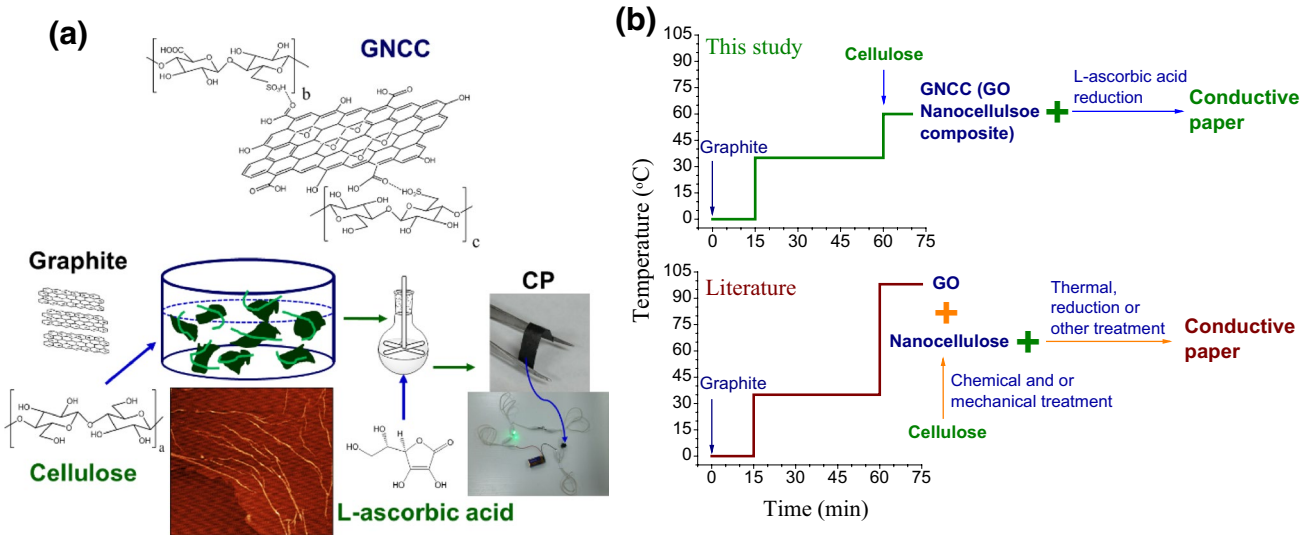

Fig. 1 **a** A schematic flow diagram illustrates GNCC production using the present one-pot method, and further reduced to form CP. **b** A comparison of the present one-pot process with the conventional approach in literature

(Table 1). In the meantime, 2 g in oven dry (OD) weight of air-dried BEP fibers was directly added into the flask and mechanically mixed (Fig. 1b) to achieve one-pot GNCC production. During this step, the BEP fibers were reacted (hydrolyzed and oxidized) in the flask for 10 min. Then the reaction was quenched by mixing 70 mL of hydrogen peroxide (2 wt%) into the flask. Any solid product (GNCC) from the reaction was separated through centrifugation at 10,000 rpm (16,270×*g*) for 10 min (Sorval RC 5B plus, DU Pont Company, Wilmington, Delaware). The collected solids were dialyzed using a membrane with typical cut-off molecular weight = 14,000 Da (D9402, Sigma-Aldrich, St Louis, MO) against DI water for 5–7 days, to result in GNCC in suspension. Figure 1b illustrates the difference between the present one-pot approach and literature conventional approach [6, 7]. In addition, various runs with different experimental conditions including the two controls to produce hydrolyzed cellulose (HCel) (Fig. S1) without adding graphite and graphene oxide (GO, Fig. S2) without adding cellulose using the standard Hummers method were carried out as listed in Table 1.

Reduction of GNCC and CP Production

GNCC suspension of 40 mL at 10 g L^{-1} was sonicated for 30 min and diluted to 92 mL with DI water in a 250-mL flask. The diluted GNCC suspension was added with 8 mL of ammonia solution (30 wt%) and 2.8 g of L-ascorbic acid under agitation. Then the mixture was immediately heated to 95 ± 3 °C and maintained for 24 h. Reduced GO (RGO) as a control was also produced in a similar procedure using GO suspension, and glucose as the reducing agent.

CP was formed by ultrafiltrating the resultant RGNCC suspension under air pressure of 586 kPa through the Millipore PVDF membrane (Millipore Corporation, USA) as described previously [24]. Both GNCC paper and GO paper were also prepared by ultrafiltration. All suspensions contain 0.4 g solids (OD weight). After filtration, the wet film was stacked between blotter papers to absorb water. The assembly was then sandwiched between two steel plates, and a 25 kg weight was place on the plates to minimize deformation (changed blotter paper every day) at room temperature for 7 days. Then the dried GNCC and CP were obtained for subsequent characterizations.

Characterizations

Fourier transform infrared (FTIR) absorption was measured using a FTIR spectrophotometer (Spectrum 100, PerkinElmer Inc., Norwalk, CT) equipped with a universal attenuated total reflectance probe in the wavenumber range of 400–4000 cm^{-1}.

Raman spectra were obtained on a Raman Spectrometer (LabRam Aramis, HJY, Inc., France) in the frequency range of 400–3500 cm^{-1} with a resolution of 1 cm^{-1}.

Static water contact angle was measured using an optical tension meter (Attension Theta Lite, Biolin Scientific Co. Ltd., Sweden) to signify the surface hydrophilicity of paper-based materials. During the test, a DI water droplet was dripped onto the surface of each sample from a microsyringe with a stainless steel needle. All samples were air dried at room temperature overnight in advance.

Zeta potential analysis was performed on a zeta-potential analyzer (Nanobrook Omni, Brookhaven Instruments, Holtsville, NY) using phase analysis light scattering (PALS) mode. To reduce error, reported results were obtained by averaging 6 measurements.

Atomic force microscopy (AFM) was used to study sample morphology (AFM workshop, Signal Hill, CA). For each sample, a drop of suspension of 0.1 g L^{-1} was deposited

Table 1 List of conditions of all one-pot experiments along with the control cellulose hydrolysis run without adding graphite, and the graphene oxide run prepared by standard Hummers method

Paper sample	Interme-diator	Graphite (g)	DI water (mL)	H_2SO_4 (wt%)	BEP fiber (g)	T (°C)	Conductivity (S m^{-1})
GO paper	GO	0.5	23.00	47.9	0	98	8.3×10^{-4}
HCelP	HCel	0	23.00	47.9	2	60	NM
CP-T60	GNCC	0.5	23.00	47.9	2	60	116.3 ± 1.5
CP_{25}-T60[a]	GNCC	0.5	23.00	47.9	1.5	60	NA
CP_{17}-T60[a]	GNCC	0.5	23.00	47.9	2.5	60	109.8 ± 12.2
CP-T60Sl	GNCC	0.5	28.75	42.4	2	60	18.8 ± 0.3
CP-T60Sll	GNCC	0.5	34.50	38.0	2	60	NM
CP-T50	GNCC	0.5	23.00	47.9	2	50	60.5 ± 0.7
CP-T50Sh	GNCC	0.5	17.25	55.1	2	50	7.3 ± 0.7

Initial H_2SO_4 concentration was 98 wt% for all runs

NA CP was not made, *NM* not measured

[a]Subscript "17" and "25" represent graphene content in wt%

onto a fresh mica and air dried overnight at ambient environment. Topographical images were taken in tapping mode at 160–225 kHz using a tip with a radius of curvature 10–15 nm. The height distribution of a sample was analyzed using Gwyddion (Dept. of Nanometrol, Czech Metrology Institute, 64-bit) equipped with the AFM.

The morphologies (of both surface and cross section) of GO paper, GNCC paper, and CP were also observed using scanning electron microscopy (SEM, Leo EVO 40, Carl Zeiss NTS, Peabody, MA). Samples were prepared by drying a certain amount of suspension (for surface probe) on a well-polished aluminum mount. For the cross section examination, specimen were randomly cut in the out of specimen plane direction. All surfaces to be examined were sputter-coated with thin gold layer to provide adequate conductivity.

Thermogravimetric analysis (TGA) was carried out using a Pyris 1 TGA (PerkinElmer Inc., Norwalk, CT) with temperature scanning from ambient to 600 °C at a heating rate of 10°C min^{-1}. After air drying at 50 °C for 4 h, approximately 4 mg of sample was used for each test. High purity nitrogen gas purge was introduced at a flow rate of 20 mL min^{-1} to prevent any unwanted oxidation.

A dynamic mechanical analyzer (DMA, Q800, TA Instruments, New Castle, DE) was utilized to determine the mechanical properties of paper samples. All samples were conditioned at 20 °C and 68–70% relative humidity for at least 7 days in advance. Then each paper strip, measuring 20 mm × 7 mm × 0.1 mm, was preloaded to a static force of 0.001 N on a tension clamp and equilibrated at 30 °C for 5 min. The applied static force was increased to allow a strain rate of 0.01% per min until 0.50% of strain was reached or the strip was fractured. For each sample, three strips were tested to report the average, and all data were analyzed using the TA Universal Analysis v4.4A software.

Electric Conductivity Measurements

The electrical conductivity of each sample in 1.5 × 1.5 (cm) was determined according to the sheet resistivity measurement using four point probing equipment (AFPP 300 upg, Superior Electronics, Phoenix, AZ). Specifically, the conductivity (S m^{-1}) was calculated in accordance with the following equation [25]:

$$\text{Conductivity} = \frac{1}{R_s \times t} \quad (1)$$

where t and R_s represent the thickness (m) and the sheet resistance (Ω^{-2}) of each specimen, respectively.

Results and Discussions

Chemical Characterization of One-pot GNCC

The one-pot process is schematically shown in Fig. 1a and compared with conventional synthesis process (Fig. 1b). Several CP were produced under different conditions and labelled as CP-Txx or CP-TxxSy (Table 1) with xx denoting hydrolysis temperature in degree C and y denoting sulfuric acid concentration either h (high 55 wt%) or l (low 42.4 wt%). The acid concentration for all CP-Txx was 48 wt%. Experimental reproducibility can be seen from the similar conductivity between CP-T60 and CP_{17}-T60 (graphene content 17 wt%). CP-T60 has the highest conductivity of 116.3 ± 1.5 S m^{-1} among all CP produced (Table 1), therefore GNCC, RGNCC, and CP produced under the condition for run CP-T60 were further characterized. In the following discussion, unless indicated otherwise, GNCC and RGNCC were referred to GNCC-T60, and RGNCC-T60, respectively. For comparison, results for GO and RGO were also presented [23].

ATR-FTIR spectra of GO, HCel, and GNCC, and CP-T60 were compared (Fig. 2a). CP-T60 has the same chemical structure as that of RGNCC, therefore, the result of CP-T60 was presented for evaluation of the reduction of GNCC by L-ascorbic acid. Obviously, all absorption peaks for GO or HCel should appear in the GNCC spectrum. However, the main feature in GO spectrum associated with C=O of carboxyl (or carbonyl) at 1732 cm^{-1} was absent from the CP-T60 spectrum, while the C=O from ketonic species at 1629 cm^{-1} was also slightly red shifted. Furthermore, a brand new peak appearing at 1554 cm^{-1} in the CP-T60 spectrum was assigned to the sp^2-hybridized C=C [26]. These suggested that the one-pot process produced GNCC, which was then successfully reduced. The high electrical conductivity of RGNCC was attributed to the restored sp^2 bonding network that arose from deoxygenation [27]. In addition, characteristic peaks around 1631 and 1732 cm^{-1}, though weak, were both observed from HCel, suggesting that cellulose was also oxidized by potassium permanganate during the one-pot process [28].

Raman spectroscopy is a powerful nondestructive technique to identify the number of layers, structure, doping, and disorder of graphene-based materials. In general, D band (1337 cm^{-1}) and G band (1601 cm^{-1}) in Raman spectra correlate to the vibration of the in-plane graphite lattice and disordered region in the graphite edges, respectively. In particular, I_D/I_G ratio, the intensity ratio between D and G band, has long been used to evaluate the degree of defects in these materials [29, 30]. As illustrated in Fig. 2b, I_D/I_G ratio values were 1.00, 1.32 and 1.27 for GO, RGO, and GNCC, respectively. The low I_D/I_G ratio

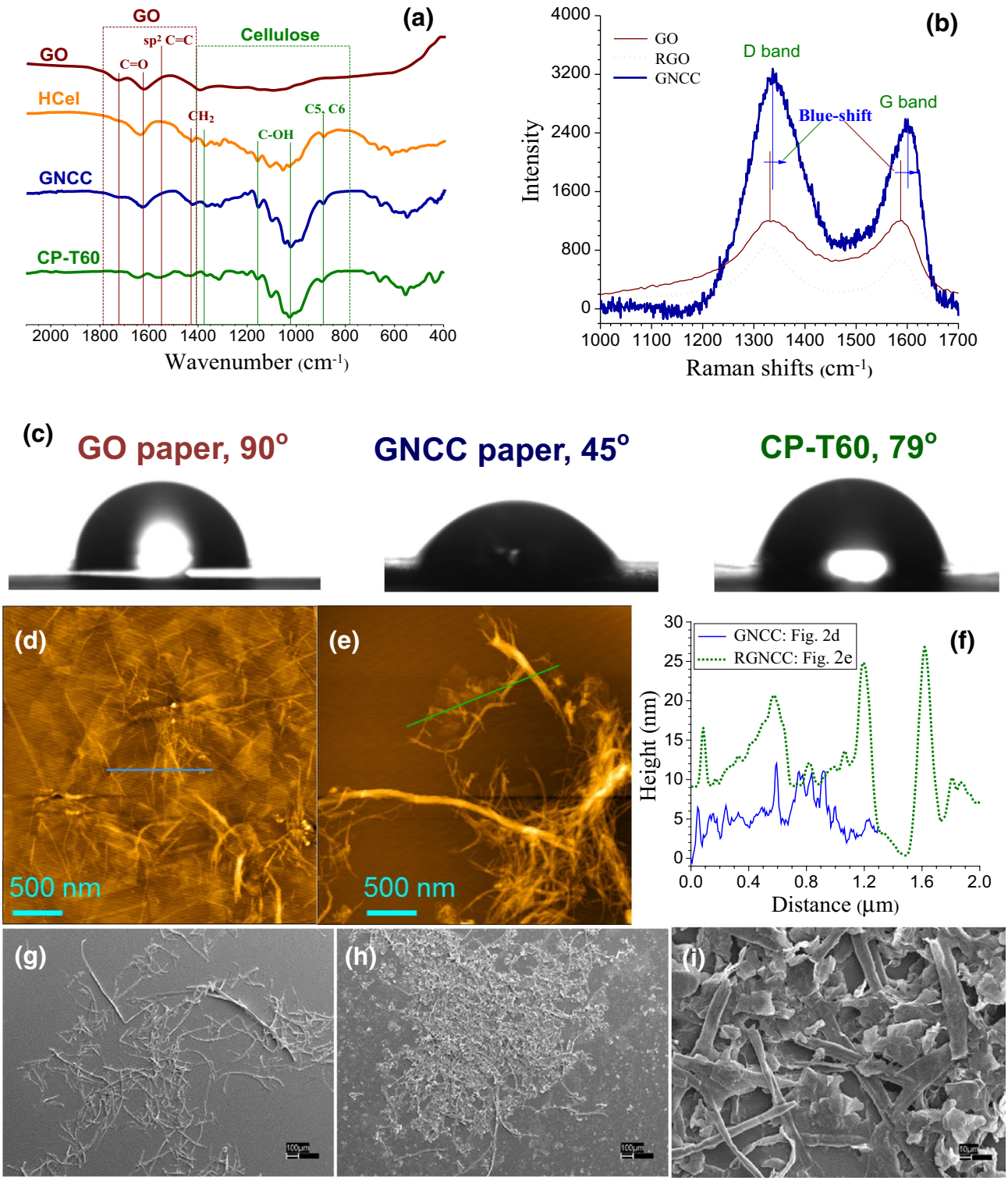

Fig. 2 **a** FTIR spectra of GO, HCel, GNCC, and CP-T60 showing typical absorption bands of GO and cellulose; **b** Raman scattering spectra of GO, RGO, GNCC; **c** static water contact angle on GO paper, GNCC paper, and CP-T60 showing L-ascorbic acid reduction reaction of GNCC to form CP restored hydrophobicity; **d** AFM images of GNCC and **e** RGNCC; **f** AFM topography measured profiles shown in **d, e; g–i** SEM images of GNCC, scale 100 μm (**g**), RGNCC, scale 100 μm (**h**), scale 10 μm (**i**)

of GO is due to the presence of oxygen from oxidation. Despite similar oxidation occurring in producing GNCC, the higher I_D/I_G ratio of GNCC suggests that it has more in-plane sp^2 domain with fewer defects than GO. This, perhaps, was due to the reductions taking place by the presence of glucose from cellulose hydrolysis using concentrated sulfuric acid [31]. Both the reduction by glucose and the slightly low temperature in oxidation (compare two schemes in Fig. 1b) resulted in improved I_D/I_G ratio with reduced defects in GNCC. This can also be seen from the blue-shift of both the D and G bands of GO compared with the corresponding bands for GNCC, implying that GNCC contains more isolated double bonds [30]. Overall, Raman characterization indicated one-pot synthesized GNCC is promising.

The degree of reduction for CP-T60 can also be assessed by comparing its static water contact angle with those of GO paper and GNCC paper (Fig. 2c). Clearly, CP-T60 with a higher water contact angle of 79° is less hydrophilic than GNCC paper, with contact angle of 45°, demonstrating that oxygen content in the CP-T60 was substantially removed by reduction using L-ascorbic acid [32]. In addition, a hydrophilic GNCC facilitates aqueous processing such as for forming paper, or in L-ascorbic acid reduction [33].

GNCC and RGNCC Morphology and Dispersity

The morphologies of GNCC and RGNCC can be clearly seen from AFM images (Fig. 2d, e). The exfoliation of graphite into GO sheets through the one-pot process can be seen from both GNCC and RGNCC. CNF with diameters less than 100 nm (Fig. 2d) and microfibrils of 10 μm (Fig. S3) were fairly well dispersed in the GNCC matrix (Fig. 2d). Improved acid hydrolysis by using either a high acid concentration > 48 wt%, or an elevated temperature for an extended reaction time in addition to enhanced mechanical mixing can reduce the size of the cellulose fibrils to be more in nanoscale as we demonstrated previously [21, 22]. The AFM height profiles suggest that GO sheets in GNCC and RGNCC were approximately 5–10 nm (Fig. 2f), or 5–10 layers of graphene. It is expected that this good exfoliation of graphite can result in good conductivity of CP produced through ultrafiltration of RGNCC [34]. It is also noticed that the dispersion of CNF became relatively difficult in RGNCC (Fig. 2e) compared with that in GNCC, perhaps due to its relatively hydrophobic property as evidenced from the water contact angle of 79°, higher than that of GNCC (45°, Fig. 2c). This is further verified by SEM images (Fig. 2g–i) that shows the differences between microfibrils in GNCC and RGNCC.

The aggregation of CNF in RGNCC may result in increased interlayer distance between GO sheets to prevent island growth of GO (Fig. 2i) [35]. SEM images also revealed that a substantial amount of microfibrils exist in GNCC and RGNCC (Fig. 2g, h), indicating that mechanical mixing applied in the one-pot process was not sufficient to fibrillate all cellulose fibers into nanofibrils. The zeta potentials of GNCC, GO, and RGNCC, however, did not show significant difference (Table S1). It should be noted that the particles in GNCC, GO, and RGNCC are not spherical, which can affect the measured charge using the Zeta-potential method based on the electrophoretical mobility of spherical particles.

Characterizations of GNCC Paper and CP

Images of GO, GNCC paper, and CP-T60 are shown in Fig. 3a–d. The two-sidedness of GNCC paper (Fig. 3b, c) is obvious due to the application of ultrafiltration for paper forming that resulted in the precipitation of GO in the bottom of the sheet molder. The relatively hydrophobic nature of RGNCC suspension through reduction using L-ascorbic acid eliminated the two-sidedness in CP (Fig. 3d). The surface and cross-sectional morphology of GO, GNCC paper, and CP-T60 were elucidated using SEM (Fig. 3e–j). The GO paper has a smooth top surface (Fig. 3e) and thin-layered structure in the cross-sectional direction (Fig. 3h). The good dispersion of cellulose fibrils in GNCC paper is apparent as no individual cellulose fibrils can be seen from the GNCC paper top surface (Fig. 3f) though it has a flower pattern, which most likely resulted from the presence of cellulose fibrils. Meanwhile, the presence of cellulose fibrils cross-linked GO sheets can be clearly seen in the GNCC paper cross-sectional direction (Fig. 3i). Due to the hydrophobic property of RGNCC through reduction that resulted in comparatively poor dispersion of cellulose fibrils, CP-T60 has very different surface (Fig. 3g) and cross-sectional (Fig. 3j) morphologies. The microfibrils can be clearly seen from the CP-T60 surface, as well as layered structure in micro-size (Fig. 3j). Unlike GNCC paper, CP-T60 contains many voids (Fig. 3g, j), which is in agreement with a previous study [4]. The porous structure can be desirable for many applications such as supercapacitors due to improved ion and charge transfer [36].

As summarized in Table 2, conventional Hummer's method prepared GO with reduction by L-ascorbic acid resulted in a conductivity of 9960 S m^{-1}, while higher values, as high as 12,000 S m^{-1}, were obtained by employing electrochemical reduction [10, 37]. However, conductivities obtained from reported GNCC were low and depended on the loading of cellulose [10]. For example, the conductivity of a RGNCC paper with CNF content of 90% was only 15.4 S m^{-1} [38]. Surprisingly, it was found that the reduction in conductivity with the decrease in graphene content was approximately linear initially and then decreased exponentially [10]. For instance, conductivity was reduced from

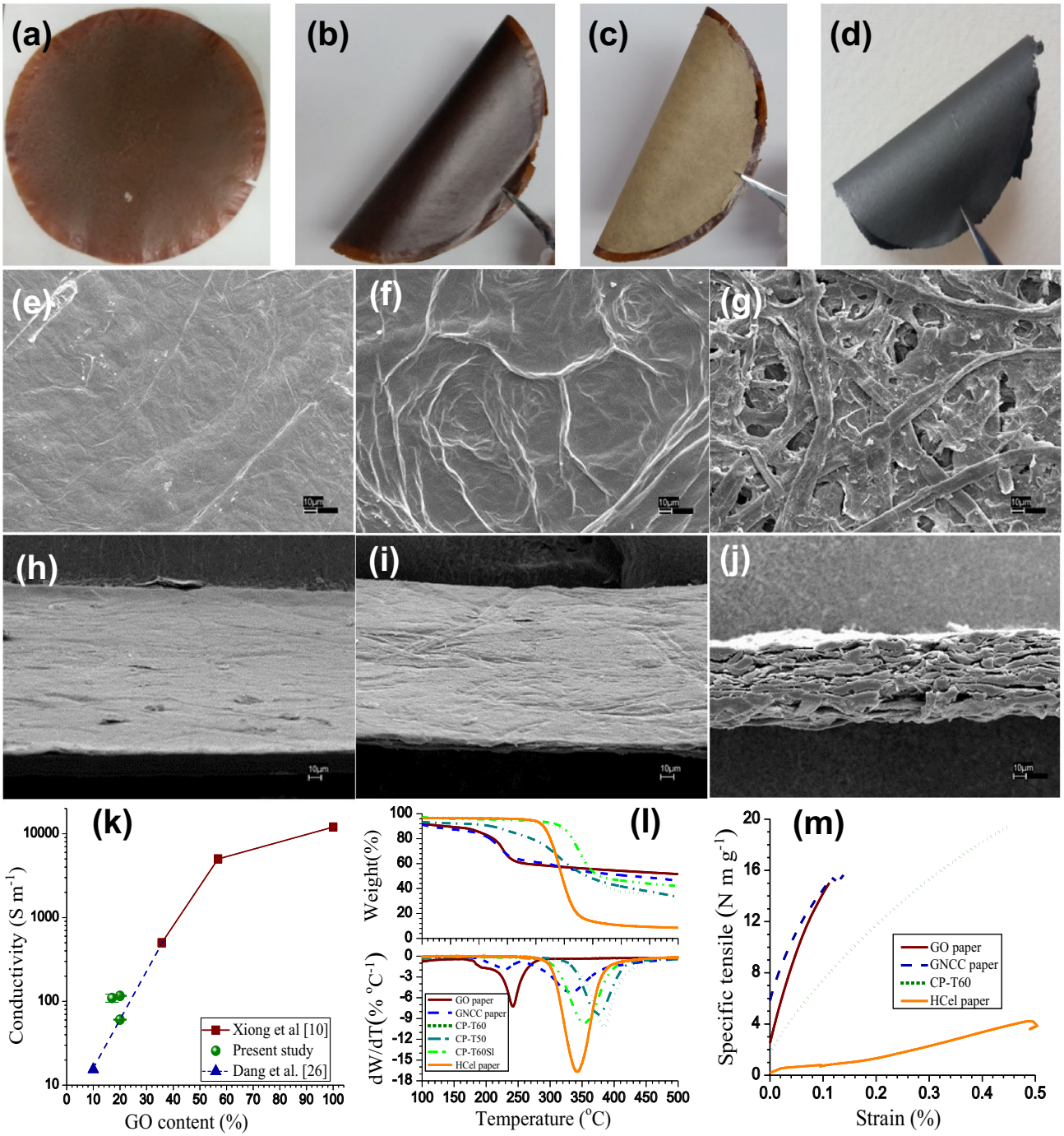

Fig. 3 Photos of GO paper (**a**), GNCC paper (**b, c**), and CP-T60 (**d**); SEM images (second panel shows top view, third panel shows cross sectional view): GO paper (**e, h**), GNCC paper (**f, i**), and CP-T60 (**g, j**); comparisons of CP conductivity with literature data (**k**); comparisons of thermal stability (**l**); DMA (**m**) conducted at 25 °C and relative humidity 68–70%

12,000 to 5000 S m^{-1} when GO content was reduced from 100 to 56.8%. Further reduction in GO to 35.7% resulted in a conductivity of only 500 S m^{-1} (a reduction by a factor of 10). This, perhaps, was due to percolation phenomenon, or a percolation graphene content of approximately 57%. We overlaid the conductivity data from Xiong et al. [10], Dang and Seppälä [38], and from the present study to illustrate this percolation phenomenon, as shown in Fig. 3k. The results clearly show the percolation point and the exponential reduction in conductivity as graphene content was reduced below the percolation point. It is noteworthy that the reduction in conductivity follows the same trend even though these data

Table 2 Comparison of electrical conductivity of CP-T60 with those graphene–cellulose composites reported in the literatures with GO paper, GNCC paper

Source	Sample	Method[a]	Cellulose content (%)	Graphene content (%)	Conductivity (S m^{-1})
[37]	Film	H + L-ascorbic acid reduction	0	100	9960
[39]	Fiber	H + mix + wet spinning + HI reduction	CNF = 9.1	90.9	8300
[10]	Membrane	H + spin coating + electrochemical reduction	CNC = 0	100	12,000
[10]	Membrane		CNC = 38.9	56.8	5000
[10]	Membrane		CNC=64.3	35.7	500
[38]	Paper	H + mix + hydrazine reduction	CNF = 90	10	15.4
This study	GO paper	H	0	100	8.3×10^{-4}
This study	GNCC paper	One-pot	Bleached fiber = 80	20	1.4×10^{-4}
This study	CP-T60	One-pot + L-ascorbic acid reduction	Bleached fiber = 80	20	116.3 ± 1.5

[a]H stands for Hummers method [13]

Table 3 TGA of the GO paper, Hcel paper, GNCC paper, and CP-T60, conducted at a heating rate of 10 °C min^{-1}

	T_{onset} (°C)	Weight at T_{onset} (%)	T_5 (°C)
GO paper	183.2	87.9	73.9
HCel paper	296.3	94.5	289.8
GNCC paper	205.4	96.3	215.7
CP-T60	319.1	91.8	261.2
CP-T60Sl	300.5	91.75	207.9
CP-T50	329.0	92.56	262.1
CP-T50Sh	321.3	90.53	246.6

T_{onset} was the temperature at which the weight loss was 1% for 1 °C increase in temperature; while T_5 is the temperature at which weight loss reached 5%

Table 4 Tensile modulus of GO paper, GNCC paper, and CP measured at 25 °C and relative humidity of 68–70%

	Tensile modulus (MPa)
GO paper	17267 ± 136.7
HCel paper	337 ± 3.9
GNCC paper	17854 ± 244.5
CP-T60	6047 ± 93.0
CP-T60Sl	716.4 ± 2.39
CP-T50	6190 ± 87.23
CP-T50Sh	1378 ± 48.88

were obtained from different studies using different reduction chemistry. The conductivity of CP from the present one-pot process is slightly higher than the trend line. This indicates that the present one-pot process was as efficient as or slightly better (Fig. 3k) than those reported in the literature [10, 38] even without optimization. The three data points shown from the present study at graphene content 17–20% also demonstrate the good reproducibility of the present one-pot process.

To demonstrate the conductive nature of the CP produced, a simple electronic circuit containing a LED light, a switch, and a 9 V DC battery was set up. The circuit contains a strip of CP with dimension of 20 × 7 mm (approximately 0.1 mm in thickness). When the battery was switched on, the LED light shining. Two LED lights with different frequencies (green and red color) were tested (Fig. S4).

TGA analyses of GO paper, GNCC paper, and CP were conducted. CP produced from different conditions did not show substantial differences (Fig. 3l). T_{onset} and T_5 were used to compare the thermal stability among GO paper, GNCC paper, and CP-T60 [13]. As listed in Table 3, CP-T60 had the highest T_{onset} of 319 °C, compared with 183 and 205 °C for GO paper and GNCC paper, respectively. This agrees with the characterization using T_5 defined as the temperature at which weight loss of 5%, i.e., T_5 was 261 °C, 74 °C, and 216 °C for CP-T60, GO paper, and GNCC paper, respectively. Major mass losses that occurred between 200 and 250 °C observed from GO and GNCC paper were due to the release of CO_2 and CO from pyrolysis of oxygen-rich groups; while decomposition above 300 °C was related to cellulose loss [13, 40, 41]. The removal of oxygen by L-ascorbic acid reduction was confirmed by the absent mass loss within 200–250 °C for all CPs.

The stress and strain curves from DMA of GO paper, GNCC paper, and CP-T60 are shown in Fig. 3m with tensile modulus listed in Table 4. CP-T60 has a strain at failure of 0.5% compared with 0.13% for GNCC paper. CP-T60 has the highest specific tensile of 19 N mg^{-1} among all samples. In short, CP-T60 from reduction not only has a higher tensile than GNCC, but also has a higher strain at break, or toughness. The fact that GO is brittle illustrates that the inclusion of cellulose in CP-T60 plays an important role in enhancing mechanical properties especially after reduction.

The improved mechanical properties are the direct result of the strong hydrophobic interactions between cellulose glucopyranose CH groups and the graphene π electron system, along with the CH–π interaction resulting from the reorientation of cellulose due to the affinity between the cellulose hydroxyl groups with the graphene π electron system [42]. This CH–π interaction is competitive with cohesive intercellulose energies. This improvement is advantageous for CP applicable in flexible electronics [4, 43, 44].

Conclusions

A facile one-pot process was developed for the production of graphene–nanocellulose conductive paper. In this process, graphene oxide and cellulose were produced in one pot and subsequently reduced by green L-ascorbic acid. CP produced through ultrafiltration exhibited excellent conductivity of 116.3 ± 1.5 S m^{-1} at 20% graphene oxide loading. This level of conductivity is in agreement with literature data of graphene cellulose paper produced using multiple steps that involves utilization of toxic chemicals and costly operations. The CP also has great thermal stability in T_{onset} of 319 °C, as well as mechanical strength with a specific tensile of 19 N mg^{-1}.

Acknowledgements We acknowledge the financial support from US Forest Service, USDA Agriculture and Food Research Initiative (AFRI) Competitive (Grant No. 2011-67009-20056), and the Chinese Scholarship Council (CSC) that made the visiting appointments of Wang and Ma at the Forest Products Laboratory possible.

References

1. Jung YH, Lee J, Qiu Y, Cho N, Cho SJ, Zhang H, Lee S, Kim TJ, Gong S, Ma Z (2016) Stretchable twisted-pair transmission lines for microwave frequency wearable electronics. Adv Funct Mater 26(26):4635–4642
2. Li L, Wu Z, Yuan S, Zhang X-B (2014) Advances and challenges for flexible energy storage and conversion devices and systems. Energy Environ Sci 7(7):2101–2122
3. Wang R, Chen L, Zhu J, Yang R (2017) Tailored and integrated production of carboxylated cellulose nanocrystals (CNC) with nanofibrils (CNF) through maleic acid hydrolysis. ChemNanoMat 3(5):328–335
4. Weng Z, Su Y, Wang DW, Li F, Du J, Cheng HM (2011) Graphene–cellulose paper flexible supercapacitors. Adv Energy Mater 1(5):917–922
5. Gao K, Shao Z, Li J, Wang X, Peng X, Wang W, Wang F (2013) Cellulose nanofiber–graphene all solid-state flexible supercapacitors. J Mater Chem A 1(1):63–67
6. Ye Y-S, Zeng H-X, Wu J, Dong L-Y, Zhu J-T, Xue Z-G, Zhou X-P, Xie X-L, Mai Y-W (2016) Biocompatible reduced graphene oxide sheets with superior water dispersibility stabilized by cellulose nanocrystals and their polyethylene oxide composites. Green Chem 18(6):1674–1683
7. Du X, Zhang Z, Liu W, Deng Y (2017) Nanocellulose-based conductive materials and their emerging applications in energy devices—review. Nano Energy 35:299–320
8. Ouyang W, Sun J, Memon J, Wang C, Geng J, Huang Y (2013) Scalable preparation of three-dimensional porous structures of reduced graphene oxide/cellulose composites and their application in supercapacitors. Carbon 62:501–509
9. Li Y, Zhu H, Shen F, Wan J, Han X, Dai J, Dai H, Hu L (2014) Highly conductive microfiber of graphene oxide templated carbonization of nanofibrillated cellulose. Adv Funct Mater 24(46):7366–7372
10. Xiong R, Hu K, Grant AM, Ma R, Xu W, Lu C, Zhang X, Tsukruk VV (2016) Ultrarobust transparent cellulose nanocrystal–graphene membranes with high electrical conductivity. Adv Mater 28(7):1501–1509
11. Wang QQ, Zhu JY, Gleisner R, Kuster TA, Baxa U, McNeil SE (2012) Morphological development of cellulose fibrils of a bleached eucalyptus pulp by mechanical fibrillation. Cellulose 19(5):1631–1643
12. Saito T, Nishiyama Y, Putaux JL, Vignon M, Isogai A (2006) Homogeneous suspensions of individualized microfibrils from TEMPO-catalyzed oxidation of native cellulose. Biomacromolecules 7(6):1687–1691
13. Chen L, Zhu J, Baez C, Kitin P, Elder T (2016) Highly thermal-stable and functional cellulose nanocrystals and nanofibrils produced using fully recyclable organic acids. Green Chem 18(13):3835–3843
14. Qin Y, Qiu X, Zhu JY (2016) Understanding longitudinal wood fiber ultra-structure for producing cellulose nanofibrils using disk milling with dilute acid prehydrolysis. Sci Rep 6:35602
15. Zhu H, Luo W, Ciesielski PN, Fang Z, Zhu JY, Henriksson G, Himmel ME, Hu L (2016) Wood-derived materials for green electronics, biological devices, and energy applications. Chem Rev 116(16):9305–9374
16. Nickerson RF, Habrle JA (1947) Cellulose intercrystalline structure. Ind Eng Chem 39:1507–1512
17. Rånby BG (1951) The colloidal properties of cellulose micelles. Discuss Faraday Soc 11:158–164
18. Mukherjee SM, Woods HJ (1953) X-ray and electron microscope studies of the degradation of cellulose by sulphuric acid. Biochim Biophys Acta 10:499–511
19. Hamad WY, Hu TQ (2010) Structure–process–yield interrelations in nanocrystalline cellulose extraction. Can J Chem Eng 88:392–402
20. Chen L, Wang Q, Hirth K, Baez C, Agarwal UP, Zhu JY (2015) Tailoring the yield and characteristics of wood cellulose nanocrystals (CNC) using concentrated acid hydrolysis. Cellulose 22:1753–1762
21. Wang Q, Zhu J, Reiner R, Verrill S, Baxa U, McNeil S (2012) Approaching zero cellulose loss in cellulose nanocrystal (CNC) production: recovery and characterization of cellulosic solid residues (CSR) and CNC. Cellulose 19(6):2033–2047
22. Wang Q, Zhu J, Considine JM (2013) Strong and optically transparent films prepared using cellulosic solid residue recovered from cellulose nanocrystals production waste stream. ACS Appl Mater Interfaces 5(7):2527–2534
23. Hummers WS Jr, Offeman RE (1958) Preparation of graphitic oxide. JACS 80(6):1339–1339
24. Wang W, Sabo RC, Mozuch MD, Kersten P, Zhu JY, Jin Y (2015) Physical and mechanical properties of cellulose nanofibril films from bleached eucalyptus pulp by endoglucanase treatment and microfluidization. J Polym Environ 23:551–558
25. Kulkarni A, Schulz KH, Lim T, Khan M (1999) Dependence of the sheet resistance of indium-tin-oxide thin films on grain size and grain orientation determined from X-ray diffraction techniques. Thin Solid Films 345(2):273–277

26. Acik M, Lee G, Mattevi C, Chhowalla M, Cho K, Chabal Y (2010) Unusual infrared-absorption mechanism in thermally reduced graphene oxide. Nat Mater 9(10):840–845
27. Dreyer DR, Park S, Bielawski CW, Ruoff RS (2010) The chemistry of graphene oxide. Chem Soc Rev 39(1):228–240
28. Roman M, Winter WT (2004) Effect of sulfate groups from sulfuric acid hydrolysis on the thermal degradation behavior of bacterial cellulose. Biomacromolecules 5(5):1671–1677
29. Reich S, Thomsen C (2004) Raman spectroscopy of graphite. Philos Trans R Soc A 362(1824):2271–2288
30. Kudin KN, Ozbas B, Schniepp HC, Prud'Homme RK, Aksay IA, Car R (2008) Raman spectra of graphite oxide and functionalized graphene sheets. Nano Lett 8(1):36–41
31. Wang Q, Zhao X, Zhu JY (2014) Kinetics of strong acid hydrolysis of a bleached kraft pulp for producing cellulose nanocrystals (CNCs). Ind Eng Chem Res 53(27):11007–11014
32. Feng H, Cheng R, Zhao X, Duan X, Li J (2013) A low-temperature method to produce highly reduced graphene oxide. Nat Commun 4:1539
33. Li D, Müller MB, Gilje S, Kaner RB, Wallace GG (2008) Processable aqueous dispersions of graphene nanosheets. Nat Nanotechnol 3(2):101–105
34. Eda G, Fanchini G, Chhowalla M (2008) Large-area ultrathin films of reduced graphene oxide as a transparent and flexible electronic material. Nat Nanotechnol 3(5):270–274
35. Geim AK, Grigorieva IV (2013) Van der Waals heterostructures. Nature 499(7459):419–425
36. Zhang LL, Zhao X, Stoller MD, Zhu Y, Ji H, Murali S, Wu Y, Perales S, Clevenger B, Ruoff RS (2012) Highly conductive and porous activated reduced graphene oxide films for high-power supercapacitors. Nano Lett 12(4):1806–1812
37. Fernández-Merino MJ, Guardia L, Paredes J, Villar-Rodil S, Solís-Fernández P, Martínez-Alonso A, Tascon J (2010) Vitamin C is an ideal substitute for hydrazine in the reduction of graphene oxide suspensions. J Phys Chem C 114(14):6426–6432
38. Dang LN, Seppälä J (2015) Electrically conductive nanocellulose/graphene composites exhibiting improved mechanical properties in high-moisture condition. Cellulose 22(3):1799–1812
39. Jiang H, Yang W, Chai S, Pu S, Chen F, Fu Q (2016) Property enhancement of graphene fiber by adding small loading of cellulose nanofiber. Nanocomposites 2(1):8–17
40. Acik M, Mattevi C, Gong C, Lee G, Cho K, Chhowalla M, Chabal YJ (2010) The role of intercalated water in multilayered graphene oxide. ACS Nano 4(10):5861–5868
41. Zhang X, Liu X, Zheng W, Zhu J (2012) Regenerated cellulose/graphene nanocomposite films prepared in DMAC/LiCl solution. Carbohydr Polym 88(1):26–30
42. Alqus R, Eichhorn SJ, Bryce RA (2015) Molecular dynamics of cellulose amphiphilicity at the graphene–water interface. Biomacromolecules 16(6):1771–1783
43. Liu R, Liang S, Tang X-Z, Yan D, Li X, Yu Z-Z (2012) Tough and highly stretchable graphene oxide/polyacrylamide nanocomposite hydrogels. J Mater Chem 22(28):14160–14167
44. Dikin DA, Stankovich S, Zimney EJ, Piner RD, Dommett GH, Evmenenko G, Nguyen ST, Ruoff RS (2007) Preparation and characterization of graphene oxide paper. Nature 448(7152):457–460